GEOPHYSICS, VOL. 72, NO. 1 (JANUARY-FEBRUARY 2007); P. E27–E32, 2 FIGS., 2 TABLES.
10.1190/1.2399445

A laboratory study to determine the effect of iron oxides on proton NMR measurements

Kristina Keating[1] and Rosemary Knight[1]

ABSTRACT

Using laboratory methods, we investigate the effect of the presence and mineralogic form of iron on measured proton nuclear magnetic resonance (NMR) relaxation rates. Five samples of quartz sand were coated with ferrihydrite, goethite, hematite, lepidocrocite, and magnetite. The relaxation rates for these iron-oxide-coated sands saturated with water were measured and compared to the relaxation rate of quartz sand saturated with water. We found that the presence of the iron oxides led to increases in the relaxation rates by increasing the surface relaxation rate. The magnitude of the surface relaxation rate was different for the various iron-oxide minerals because of changes in both the surface-area-to-volume ratio of the pore space, and the surface relaxivity. The relaxation rate of the magnetite-coated sand was further increased because of internal magnetic field gradients caused by the presence of magnetite. We conclude that both the concentration and mineralogical form of iron can have a significant impact on NMR relaxation behavior.

INTRODUCTION

Proton nuclear magnetic resonance (NMR) has been widely used in the geophysical and medical communities to detect the presence of hydrogen nuclei (^{1}H) and determine their physiochemical environment. NMR measurements in the earth sciences can be made in the laboratory, or in the field using a well-logging device or a system deployed at the earth's surface. NMR logging has been employed in the oil industry to quantify water and hydrocarbon content and to estimate pore size and permeability (e.g., Seevers, 1966; Timur, 1969; Korb et al., 2003). The surface-based system, referred to as MRS (magnetic resonance sounding), has been used to estimate the water content and the permeability of the top 100 m of earth (e.g., Shushakov, 1996; Legchenko et al., 2002). The use of NMR to determine the permeability of water-saturated geologic materials is the application of interest in our research.

If we consider a water-saturated geologic material, the NMR experiment (in the laboratory or in the field) consists of measuring the rate at which the bulk nuclear magnetization of the water within the sampled volume of material returns (relaxes) to equilibrium after being perturbed by a radio-frequency pulse. The measured relaxation rate is related to the surface-area-to-volume ratio of the water-filled pore space; this is the link that allows the use of NMR data to estimate pore sizes (e.g., Timur, 1969; Yaramanci et al., 2002) and permeability (e.g., Vogeley and Moses, 1992; Legchenko et al., 2002).

A complicating factor in the interpretation of NMR relaxation rates is the effect of Fe(III), a paramagnetic species commonly found in geologic material. Previous laboratory studies (Foley et al., 1996; Bryar et al., 2000) have shown conclusively that an increase in the concentration of Fe(III), in the solid phase of a geologic material, will cause an increase in the NMR relaxation rate. What has not been investigated, however, is the role of the mineralogic form of the Fe(III). That is, is it simply the concentration of Fe(III) that determines the effect of Fe(III) on NMR data, or must the mineralogic form of Fe(III) also be considered?

Publications in the medical literature clearly show that the chemical form of iron affects proton NMR relaxation rates (Yilmaz et al., 1990; Babes et al., 1998; Gossuin et al., 2002). It has been suggested, based on theoretical modeling, that differences in relaxation rates resulting from changes in the form of the iron can be attributed to the size of the particles containing the paramagnetic species, the distance of the paramagnetic species from the relaxing protons, and the distribution and concentration of the paramagnetic species (Gillis and Koenig, 1987). These results and discussion in the medical literature led us to hypothesize that the mineralogic form of Fe(III) would affect the NMR relaxation rates of water-saturated geologic materials.

Although iron can be found in many forms, we limited this study to iron-oxide minerals. We compared NMR relaxation rates for water in sands coated with known concentrations of Fe(III) in the form

Manuscript received by the Editor March 23, 2006; revised manuscript received September 2, 2006; published online December 29, 2006.
[1]Stanford University, Department of Geophysics, Mitchell Building, Stanford, California 94304. E-mail: kkeat@pangea.stanford.edu; rknight@pangea.stanford.edu.

of ferrihydrite [$Fe(OH)_3 \cdot nH_2O$], goethite (α-FeOOH), hematite (α-Fe_2O_3), lepidocrocite (γ-FeOOH), and magnetite (Fe_3O_4). These iron oxides were chosen to represent a variety of Fe(III)-bearing, naturally occurring iron minerals. The selected iron oxides are pure Fe(III) minerals, with the exception of magnetite which contains both Fe(III) and Fe(II). Understanding the effect of these iron minerals is essential if we are to use NMR data, in the laboratory or the field, to obtain accurate information about the permeability of geologic materials.

NMR RELAXATION THEORY

All atoms with an odd number of protons or neutrons possess a nuclear spin angular momentum. In many geologic applications, the hydrogen atom (^1H) with a single proton is of interest because of its presence in water. In a static magnetic field (B_0), the nuclear spins in the water align with the field, resulting in a net magnetization (M_0) which is proportional to the number of ^1H in the sample. M_0 processes at the Larmor frequency f_0, which is related to B_0 by

$$f_0 = \frac{1}{2\pi}\gamma|B_0|, \tag{1}$$

where γ is the gyromagnetic ratio for hydrogen protons in water molecules [$\gamma = 0.267$ rad/(nT·s)]. For MRS instruments, f_0 ranges from 0.8 to 2.8 kHz; for NMR well-logging instruments, f_0 ranges from 0.5 to 2 MHz; and for laboratory instruments, f_0 ranges from 0.01 to 900 MHz. If a magnetic field oscillating at f_0 is applied for a short time, the nuclear spins move away from, and then relax to, their equilibrium position. This results in a measurable signal from the bulk nuclear magnetization (M), which can be described in terms of a transverse magnetization M_{xy}, and a longitudinal magnetization M_z. Parameters that describe the observed relaxation of M_{xy} are denoted with the subscript 2, and those describing the observed relaxation of M_z are denoted with the subscript 1. In this study we measured M_{xy}, which is the parameter detected by most well-logging and surface-based NMR instruments.

For bulk fluids, the return or relaxation to equilibrium over time (t) behaves as an exponential decay:

$$M_{xy}(t) = M_0(e^{-t/T_{2B}}), \tag{2}$$

where T_{2B} is the bulk fluid relaxation time; the inverse, T_{2B}^{-1}, is referred to as the bulk fluid relaxation rate and results from dipole-dipole molecular interactions. The magnitude of T_{2B}^{-1} for a fluid depends on the viscosity via the reduction of rotational mobility, the concentration of dissolved paramagnetic species such as dissolved oxygen, Mn^{2+} ions, or Fe^{3+} ions, and pH (Bloembergen et al., 1948; Bryar et al., 2000).

The relaxation rate of water in a porous material is generally found to be greater than T_{2B}^{-1} because of two other mechanisms that can enhance relaxation. The relaxation rate of water in a pore T_2^{-1} (where T_2 is the relaxation time), is described as a sum of three relaxation rates (Brownstein and Tarr, 1979):

$$T_2^{-1} = T_{2B}^{-1} + T_{2s}^{-1} + T_{2D}^{-1}, \tag{3}$$

where T_{2S}^{-1} is the surface relaxation rate and T_{2D}^{-1} is the diffusion relaxation rate (T_{2S} and T_{2D} are the surface and diffusion relaxation times.) The surface relaxation rate is determined by the interaction that occurs between the water protons and paramagnetic sites on the solid surface of the pore space. In the case of fast diffusion, which assumes that all protons travel to and relax at the solid surface in the time interval of the NMR experiment, the surface relaxation rate is given by (Senturia and Robinson, 1970; Brownstein and Tarr, 1979)

$$T_{2s}^{-1} = \rho_2\frac{S}{V}, \tag{4}$$

where S/V is the surface-area-to-volume ratio of the water-filled pore and ρ_2 is the surface relaxivity. The diffusion relaxation rate is determined by the effect of the magnetic properties of the solid on the diffusing water molecules. The diffusion relaxation rate T_{2D}^{-1} is related to the average internal gradient of the magnetic field (G) and the diffusion coefficient of water (D) by

$$T_{2D}^{-1} = \frac{D}{12}(\gamma G t_E)^2, \tag{5}$$

where γ is the gyromagnetic ratio, and t_E is the echo time—a rephasing parameter used during the Carr-Purcell-Meiboom-Gill (CPMG) pulse sequence. The CPMG pulse sequence (Carr and Purcell, 1954; Meiboom and Gill, 1958) was developed to rephase proton spins in a solid in the presence of nonuniform magnetic fields. The average internal gradient of the magnetic field is caused by the magnetic susceptibility of each phase in the geologic material, and by the differences in susceptibility between the phases. Ferrihydrite, goethite, hematite, and lepidocrocite are antiferromagnetic minerals with magnetic susceptibilities ranging from 0.5×10^{-3} to 40×10^{-3} SI. Magnetate is a ferrimagnetic mineral with a magnetic susceptibility ranging from 1000×10^{-3} to 5700×10^{-3} SI. Quartz and water are both diamagnetic, with the magnetic susceptibility of quartz ranging from -13×10^{-6} to -17×10^{-6} SI, and the magnetic susceptibility of water equal to -9×10^{-6} SI (Hunt et al., 1995; Cornell and Schwertmann, 2003).

When water saturates a geological material with a range of pore sizes, a multiexponential decay is observed,

$$M(t) = \sum_i m_i e^{-t/T_{2i}}, \tag{6}$$

where m_i is proportional to the number of moles of ^1H relaxing with rate T_{2i}^{-1} and $M(0)$ is proportional to the total moles of ^1H. The values of m_i versus T_{2i} are often plotted to show the distribution of relaxation times. In studies of the NMR response of porous materials, the arithmetic mean of log T_2 (T_{2ML}) is typically calculated from the distribution of relaxation times and used to represent the relaxation behavior. Equation 3 then becomes

$$T_{2ML}^{-1} = T_{2B}^{-1} + T_{2s}^{-1} + T_{2D}^{-1}, \tag{7}$$

where T_{2B}^{-1}, T_{2s}^{-1}, T_{2D}^{-1} are now taken to be average values for the entire pore space of the sample material instead of a single pore. T_{2S}^{-1} is still described by equation 4, but ρ_2 and S/V are average values. Current NMR theory associates the average ρ_2 with the paramagnetic species (i.e., unpaired electrons) on the surface of the pore space within the sampled material (Brownstein and Tarr, 1979; Godefroy et al., 2001).

To investigate the effect of the mineralogic form of Fe(III) on the NMR response of a geologic material, we conducted a laboratory study to compare the magnitude of the five averaged parameters T_{2ML}^{-1}, T_{2B}^{-1}, T_{2s}^{-1}, T_{2D}^{-1}, and ρ_2, for water-saturated samples containing pure quartz and five different iron oxides, with known concentrations of Fe(III). This allowed us to quantify changes in T_{2ML}^{-1} with

changes in mineralogy and determine which relaxation mechanism (bulk fluid, surface, or diffusion) was responsible for any observed change in T_{2ML}^{-1}.

METHODS AND MATERIALS

Materials and NMR sample preparation

In order to determine the NMR response of the selected iron oxides, we prepared samples of quartz sand coated with the iron oxides. This allowed us to control the concentration of iron in the samples and prevented the iron oxides from forming aggregates. Quartz sand [99.995%, >40 mesh, silicon (IV) dioxide, Alfa Aesar] was used in this study as an analog for a naturally occurring mineral surface. The quartz sand was rinsed with 10% HCl deionized water (18 $M\Omega \cdot cm$) to remove paramagnetic species, then coated with the iron oxides: ferrihydrite, goethite, hematite, lepidocrocite, and magnetite.

The same general procedure was used to prepare quartz sand coated with ferrihydrite, goethite, hematite and lepidocrocite. First, the iron oxide was synthesized. Ferrihydrite was synthesized by the titration of $Fe(NO_3)_3 \cdot 9H_2O$ (0.4 mol/L) with 1 mol/L NaOH to pH 7 (Hansel et al., 2003); goethite was synthesized by the slow oxidation of $FeCl_2 \cdot 4H_2O$ solution (Schwertmann and Cornell, 2000); hematite was synthesized by the forced hydrolysis of $Fe(NO_3)_3 \cdot 9H_2O$ (0.4 mol/L) solution (Schwertmann and Cornell, 2000); and lepidocrocite was synthesized by the hydrolysis of $FeCl_2 \cdot 4H_2O$ (0.2 mol/L) kept at ph 6.7, using 1 mol/L NaOH (Schwertmann and Cornell, 2000). The synthesized iron oxides were then washed with deionized water to remove excess salts. Slurries composed of the synthesized iron oxides and deionized water were mixed with sand to obtain a mixture containing 1% iron by weight (calculated stoichiometrically); this mixture was allowed to dry. The iron-coated sands were subsequently washed three times with deionized water. Once coated, the mineral compositions of the synthesized iron oxides were confirmed using X-ray diffraction spectrometry.

Powdered, synthetic magnetite, in the form of synthetic iron oxide (100% Fe_3O_4, Fisher Scientific), was chosen as an analog for naturally occurring magnetite. Then we followed the same procedure used with the other iron oxides to obtain quartz sands coated with magnetite. Initially, the magnetite and sand were mixed to contain 1% iron by weight; however, the relaxation time of the 1% mixture was found to be too short to measure. A mixture of magnetite and sand containing 0.65% iron by weight was prepared and used in this study.

NMR measurement procedures

Two samples of each type of sand (pure quartz and iron-coated) were packed into cylindrical Teflon sample holders of interior diameter 2.1 cm and height 6 cm. The porosity of each sample, packed in the container, was measured with a Coberly-Steven Helium Pycnometer. Once the porosity had been measured, the sample was saturated under pressure with deionized water; this process took approximately 30 minutes. NMR measurements were made approximately 1 hour after the saturation of the samples.

NMR relaxation data were collected using a 2.2 MHz Maran Ultra NMR Core Analyzer (Resonance Instruments) using a CPMG pulse sequence. A single data point was obtained at each echo in the CPMG pulse sequence; 32,000 echoes were used. Data were collected at four echo times, t_E = 300, 400, 600, and 800 μs, resulting in total times for each pulse sequence of 9.6, 12.8, 19.2, and 25.6 s. The data were stacked 100 times to improve the signal-to-noise ratio. The delay time between each pulse sequence was 10 s to ensure that the sample had returned to thermal equilibrium prior to the start of the pulse sequence. Measurements were consistently made at 30 °C.

Once the NMR measurements had been completed on the saturated samples, the pore water was removed from each sample by centrifuging and used to measure T_{2B}^{-1}. It was only necessary to measure T_{2B}^{-1} at one value of t_E because no internal magnetic field gradient is present in fluids; we chose t_E = 300 μs as a representative echo spacing. Then, the NMR samples were dried overnight.

Three subsamples of each type of iron-coated sand were taken for surface area analysis; two of the subsamples from one NMR sample and one subsample from the other. Surface area measurements were also made on three samples of the quartz sand. The specific surface area (S_s) of each sand, defined as the surface area normalized by the mass of the sample, was measured using a Beckman-Coulter SA3100 Analyzer, which produces accurate results for samples with a total surface area of 3 m^2 or higher. For samples where S_s was less then 0.2 m^2/g, the S_s measurement was repeated using a Micromeritics ASAP 2020 Accelerated Surface Area and Porosimetry System, which produces accurate results for samples with a total surface area as low as 1 m^2. All samples were measured using the Brunauer-Emmett-Teller (BET) adsorption method with $N_2(g)$ as the adsorbate.

DATA ANALYSIS AND RESULTS

Porosity and surface area

The measured porosity and specific surface area for each sample are given in Table 1. The porosity ranged from 0.46 for the hematite-coated sand to 0.50 for the goethite-coated sand. These values are the same, within experimental error, as the porosity of the quartz sand sample (0.48) indicating that the addition of the iron coatings did not significantly change the porosity. For the sands coated with ferrihydrite, goethite, hematite, and lepidocrocite, the surface area increased significantly with the addition of the iron coating. The ferrihydrite-coated sand has a much higher surface area than the other iron-coated sands because of its amorphous crystal structure. The specific surface area of the quartz sand was not changed significantly by the addition of magnetite. S/V, also in Table 1, was calculated from

Table 1. Physical property measurements porosity (ϕ), specific surface area (S_s), and the calculated surface-area-to-volume ratio (S/V).

Material	ϕ	S_s (m^2/g)	S/V ($1/\mu m$)
Quartz sand	0.48 ± 0.02	0.15 ± 0.02	0.48 ± 0.06
Goethite-coated sand	0.50 ± 0.02	0.58 ± 0.09	1.6 ± 0.2
Lepidocrocite-coated sand	0.49 ± 0.02	0.27 ± 0.03	0.75 ± 0.08
Ferrihydrite-coated sand	0.49 ± 0.02	2.5 ± 0.5	7.3 ± 0.5
Hematite-coated sand	0.46 ± 0.02	0.35 ± 0.03	1.09 ± 0.09
Magnetite-coated sand	0.48 ± 0.02	0.19 ± 0.02	0.48 ± 0.02

$$\frac{S}{V} = m_s S_s \left(\frac{1}{V_p} \right), \tag{8}$$

where m_s is the total mass of the solid component, and V_p is the volume of the pore space. V_p was obtained from gravimetric measurements of the sample prior to and following saturation. Errors in the surface areas were calculated from repeated measurements and are attributed to the variability between samples of the same material.

Sand sample relaxation rates, T_{2ML}^{-1}

Each NMR data set, from all the sand samples, displayed a multiexponential decay of magnetization (as described by equation 6). The data were fit to a distribution of 200 exponentially spaced T_2 values ranging from 1 ms to 10 s using the regularized nonnegative least-squares inversion routine developed by Whittall et al. (1991). This approach gives a less biased interpretation of the data than other commonly used fits (e.g., single-exponential, stretched-exponential, or double-exponential) because it does not specify the number of relaxation times, but instead allows any number of relaxation times between 0 and 200. The residual of each fit was examined to ensure that the noise was Gaussian and the data had not been overfit.

The T_2 distributions for the quartz sand and the iron-coated sands are shown in Figure 1 for t_e = 300 μs. The quartz sand T_2 distribution is a single, narrow peak; the T_2 distributions for the iron-coated sands are broader. The distributions for goethite-, lepidocrocite-, and ferrihydrite-coated sand are very similar in form with one dominant peak and other smaller peaks. The distribution of the hematite-coated sand is similar in form, but the peaks are not well resolved, and the amplitude of the dominant peak is lower than seen for the other three sands. The magnetite-coated sand has multiple unresolved peaks spread over several decades but does not contain a clear dominant peak.

The relaxation time distributions were used to determine T_{2ML}^{-1} for the samples. These values for t_E = 300 μs are given in Table 2. As expected, the presence of iron in a sample always results in a value for T_{2ML}^{-1} greater than T_{2ML}^{-1} for the pure quartz sand. However, as seen in Table 2, it is not simply the amount of iron present that can explain the magnitude of T_{2ML}^{-1}. The ferrihydrite-, goethite-, hematite-, and lepidocrocite-coated sands all contained the same amount of iron, but have markedly different values for T_{2ML}^{-1}. And the magnetite-coated sand, which contained the least amount of iron, has the greatest relaxation rate. In the following sections, we compare the averaged values T_{2B}^{-1}, T_{2D}^{-1}, and T_{2S}^{-1} to determine the mechanism (bulk fluid, surface, or diffusion) by which the change in the mineralogy of the samples has affected T_{2ML}^{-1}.

Bulk fluid relaxation rates, T_{2B}^{-1}

The NMR relaxation rates for the bulk fluids, extracted from the samples, are given in Table 2. To obtain these values of T_{2B}^{-1}, the NMR relaxation data for the extracted bulk fluids were fit to a single-exponential decay using a least-squares algorithm. Analysis of the residuals indicated that a single-exponential decay was a valid assumption. The relaxation rate for deionized water was found to be 0.328 s^{-1}. The values of T_{2B}^{-1} for the fluids from the quartz sand, the goethite-coated sand, and the hematite-coated sand were the same, within experimental error, as T_{2B}^{-1} of deionized water. The T_{2B}^{-1} values for the fluids from the ferrihydrite-coated sand, the lepidocrocite-coated sand, and the magnetite sand were 0.411 s^{-1}, 0.344 s^{-1}, and 0.90 s^{-1}, respectively. The increase in T_{2B}^{-1} from that of deionized water is most likely because of the presence of dissolved paramagnetic species or suspended mineral particles.

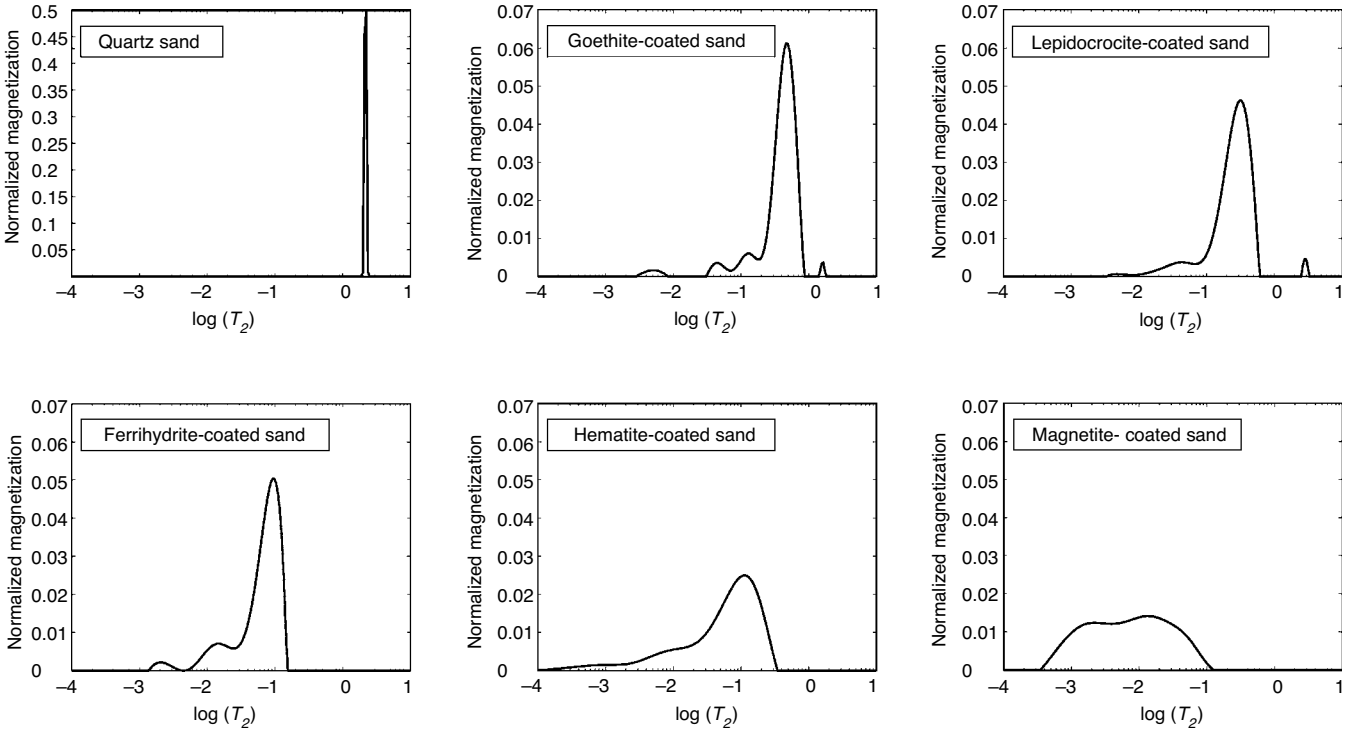

Figure 1. Normalized relaxation time distributions for quartz sand, ferrihydrite-coated sand, goethite-coated sand, hematite-coated sand, lepidocrocite-coated sand, and magnetite-coated sand.

Diffusion relaxation rates, T_{2D}^{-1}

The magnitude of the diffusion relaxation term, T_{2D}^{-1}, in the NMR response of a sample can be determined by measuring the dependence of T_{2ML}^{-1} on echo time t_E. As can be seen from equations 5 and 7, a plot of T_{2ML}^{-1} versus the square of the echo time (t_E^2) will yield a straight line with slope equal to $D(\gamma G)^2/12$. Figure 2 shows this plot for one sample of each of the iron-coated sands. The value of T_{2ML}^{-1} for the sands coated with ferrihydrite, goethite, hematite, and lepidocrocite shows negligible dependence on t_E^2, indicating that $D(\gamma G)^2/12$ from equation 5 is zero, within experimental error. Given that D and γ are nonzero, this means that $G = 0$ (i.e., there are no internal gradients in the magnetic field). The value of T_{2D}^{-1} for these samples, as given in Table 2, is zero.

T_{2ML}^{-1} for sand coated with magnetite shows a significant dependence on t_E^2. This indicates that the presence of magnetite causes internal gradients in the magnetic field ($G \neq 0$), as expected given its high magnetic susceptibility. The value of $D(\gamma G)^2/12$, obtained from the least squares fit of T_{2ML}^{-1} versus t_E^2, was used to calculate T_{2D}^{-1} according to equation 5. At $t_E = 300$ μs, the value of T_{2D}^{-1} was 17 s^{-1} as shown in Table 2. It is clear from this that the presence of magnetite will result in a significant contribution to the measured relaxation rate from the diffusion relaxation mechanism.

Surface relaxation rates, T_{2s}^{-1}

The final parameter to be assessed is the surface relaxation rate. The values of T_{2s}^{-1} determined using equation 7 for all samples are shown in Table 2. For the ferrihydrite-, goethite-, hematite-, and lepidocrocite-coated sands, and the quartz sand, T_{2s}^{-1} was calculated from equation 7 with $T_{2D}^{-1} = 0$. For the magnetite-coated sand, the relaxation rate extrapolated to $t_E^2 = 0$ (where $T_{2ML}^{-1} = T_{2B}^{-1} + T_{2s}^{-1}$) was used to calculate T_{2s}^{-1}. Values of T_{2s}^{-1} for the samples range from 0.16 s^{-1} for quartz sand to 125 s^{-1} for the magnetite-coated sand. As can be seen by reviewing these values in Table 2, it is the variation in this term that is responsible for the variation seen in the NMR relaxation rates for the samples. In fact, the magnitude of this term is very close to the magnitude of T_{2ML}^{-1} for the ferrihydrite-, goethite-, hematite-, and lepidocrocite-coated sands.

The value of T_{2s}^{-1} for a material is determined by both S/V and the surface relaxivity ρ_2. The values of S/V are given in Table 1, and the values of ρ_2, computed from T_{2s}^{-1} using equation 4, are given in Table 2. The values of ρ_2 range from 0.31 μm/s for quartz sand to 327 μm/s for magnetite-coated sand. The small ρ_2 for the quartz sand indicates that there are little to no paramagnetic species in this sand. Of specific interest is the observed variation in ρ_2 for the iron-coated sands. In this study, the variations in ρ_2 cannot be attributed to variation in the concentration of iron. The ferrihydrite-, goethite-, hematite-, and lepidocrocite-coated sands all contained an iron concentration of 1%. The magnetite-coated sand contained 0.65% magnetite and, despite its lower iron content, has a very large ρ_2 value. The variation in ρ_2 most likely reflects a difference in parameters such as the density and distribution of paramagnetic species on the surface of the pores, the distance between the relaxing protons and the paramagnetic species, and the spin quantum number associated with the paramagnetic species. These parameters have been previously shown to have an effect on ρ_2 (Godefroy et al., 2001). Identifying and quantifying the parameters that are the fundamental cause of these variations is a topic of ongoing research, and requires characterizing the hydrated surface structure of each iron-oxide mineral.

Table 2. NMR relaxation rates and calculated relaxation parameters. Both T_{2ML}^{-1} and T_{2D}^{-1} for magnetite were calculated at t_E = 300 μs.

Material	T_{2ML}^{-1} (s^{-1})	T_{2B}^{-1} (s^{-1})	T_{2S}^{-1} (s^{-1})	T_{2D}^{-1} (s^{-1})	ρ_2 (μm/s)
Quartz sand	0.49 ± 0.02	0.328 ± 0.005	0.16 ± 0.02	0	0.31 ± 0.04
Goethite-coated sand	2.9 ± 0.1	0.326 ± 0.006	2.57 ± 0.05	0	1.61 ± 0.03
Lepidocrocite-coated sand	4.4 ± 0.1	0.344 ± 0.006	4.1 ± 0.2	0	5.4 ± 0.2
Ferrihydrite-coated sand	16 ± 1	0.411 ± 0.008	16 ± 2	0	2.2 ± 0.3
Hematite-coated sand	20 ± 2	0.329 ± 0.006	19 ± 2	0	17.9 ± 0.5
Magnetite-coated sand	143 ± 19	0.90 ± 0.04	125 ± 15	17 ± 2	292 ± 5

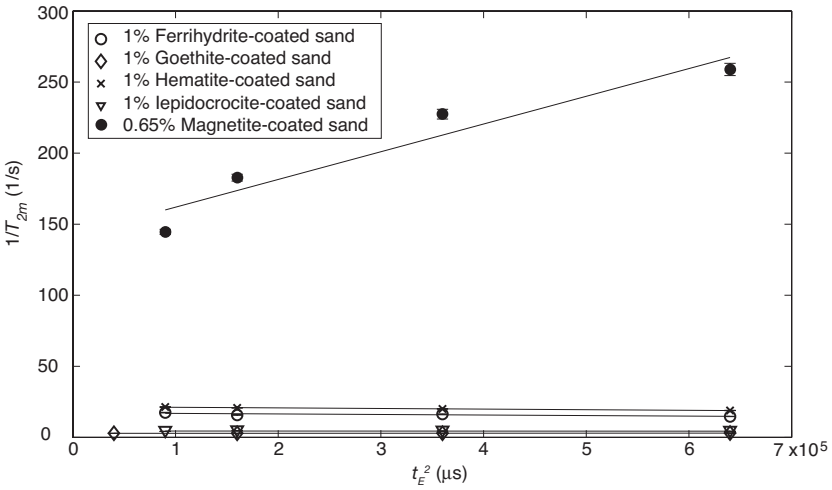

Figure 2. Plot of the transverse relaxation rate (T_{2ML}^{-1}) as a function of the square of the echo-time (t_E^2) for ferrihydrite-coated sand, goethite-coated sand, lepidocrocite-coated sand, hematite-coated sand, and magnetite-coated sand.

CONCLUSIONS

The measurements from this study show conclusively that the NMR relaxation rate of a water-saturated sand is affected by both the presence and the mineralogical form of iron. The dominant effect of ferrihydrite, goethite, hematite, lepidocrocite, and magnetite was to increase T_{2S}^{-1}, the magnitude of which is determined by S/V and ρ_2.

We found that the value of ρ_2 was very different for the different iron oxides; with additional research needed to determine the fundamental cause of these observed differences. The addition of magnetite to the quartz sand resulted in internal gradients and a contribution to T_{2ML}^{-1} from the diffusion relaxation mechanism.

In order to use NMR relaxation rates to obtain accurate estimates of permeability in geologic materials, we need to be able to account for the effects of iron-oxide minerals. Although this laboratory study has been a start, we believe that it is necessary to explore a larger range of iron minerals and to further investigate the mechanisms controlling the changes in relaxation behavior that we observed. Quantifying the physical properties of minerals that lead to variations in relaxation rates will enhance our fundamental understanding of NMR relaxation and ultimately provide improved interpretation of NMR data.

ACKNOWLEDGMENTS

We would like to thank Jim Leckie and Gordon Brown for the use of their surface area analyzers, and Kate Tufano and Matt Ginder-Vogel of the Stanford Environmental Soil and Biogeochemistry group for providing XRD measurements. We would also like to thank the associate editor for his/her handling of this paper, and the reviewers for their helpful comments. This work was supported in full by funding to Rosemary Knight under grant DE-FG02-03ER15382-A0003 from the U.S. Department of Energy.

REFERENCES

Babes, L., B. Denizot, G. Tanguy, J. J. Le Jeune, and P. Jallet, 1998, Synthesis of iron oxide nanoparticles used as MRI contrast agents: A parametric study: Journal of Colloid and Interface Science, **212**, 474–482.

Bloembergen, N., E. M. Purcell, and R. V. Pound, 1948, Relaxation effects in nuclear magnetic resonance absorption: Physical Review, **73**, 679–715.

Brownstein, K. R., and C. E. Tarr, 1979, Importance of classical diffusion in NMR studies of water in biological cells: Physical Review A, **19**, 2446–2453.

Bryar, T. R., C. J. Daughney, and R. J. Knight, 2000, Paramagnetic effects of iron(III) species on nuclear magnetic relaxation of fluid protons in porous media: Journal of Magnetic Resonance, **142**, 74–85.

Carr, H. Y., and E. M. Purcell, 1954, Effects of diffusion on free precession in nuclear magnetic resonance experiments: Physical Review, **94**, 630–638.

Cornell, R. M., and U. Schwertmann, 2003, The iron oxides: Properties, reactions, occurrences and uses: Wiley-VCH.

Foley, I., S. A. Farooqui, and R. L. Kleinberg, 1996, Effect of paramagnetic ions on NMR relaxation of fluids at solid surfaces: Journal of Magnetic Resonance, **123**, 95–104.

Gillis, P., and S. H. Koenig, 1987, Transverse relaxation of solvent protons induced by magnetized spheres: Application to ferritin, erythrocytes and magnetite: Magnetic Resonance in Medicine, **5**, 323–345.

Godefroy, S., J. P. Korb, M. Fleury, and R. G. Bryant, 2001, Surface nuclear magnetic relaxation and dynamics of water and oil in macroporous media: Physical Review E, **64**, 21605-1–13.

Gossuin, Y., A. Roch, R. N. Muller, P. Gillis, and F. Lo Bue, 2002, Anomalous nuclear magnetic relaxation of aqueous solutions of ferritin: An unprecedented first-order mechanism: Magnetic Resonance in Medicine, **48**, 959–964.

Hansel, C. M., S. G. Benner, J. Neiss, A. Dohnalkova, R. K. Kukadapu, and S. Fendorf, 2003, Secondary mineralization pathways induced by dissimilatory iron reduction of ferrihydrite under advective flow: Geochimica et Cosmochimica Acta, **67**, 2977–2992.

Hunt, C. P., B. M. Moskowitz, and S. K. Banerjee, 1995, Magnetic properties of rocks and minerals, *in* T. J. Ahrens, ed., Rock physics and phase relations: A handbook of physical constants: AGU Books Board, 189–204.

Korb, J. P., S. Godefroy, and M. Fleury, 2003, Surface nuclear magnetic relaxation and dynamics of water and oil in granular packings and rocks: Magnetic Resonance Imaging, **21**, 193–199.

Legchenko, A., J. M. Baltassat, A. Beauce, and J. Bernard, 2002, Nuclear magnetic resonance as a geophysical tool for hydrogeologists: Journal of Applied Geophysics, **50**, 21–46.

Meiboom, S., and D. Gill, 1958, Modified spin-echo method for measuring nuclear relaxation times: Review of Scientific Instruments, **29**, 688–691.

Schwertmann, U., and R. M. Cornell, 2000, Iron oxides in the laboratory: Preparation and characterization: Wiley-VCH.

Seevers, D. O., 1966, A nuclear magnetic method for determining the permeability of sandstones: Transactions of the SPWLA 7th Annual Logging Symposium, Paper L.

Senturia, S. D., and J. D. Robinson, 1970, Nuclear spin-lattice relaxation of liquids confined in porous solids: Society of Petroleum Engineers Journal, **10**, 237–244.

Shushakov, O. A., 1996, Groundwater NMR in conductive water: Geophysics, **61**, 998–1006.

Timur, A., 1969, Pulsed nuclear magnetic resonance studies of porosity, movable fluid, and permeability of sandstone: Journal of Petroleum Technology, **21**, 755–786.

Vogeley, J. R., and C. O. Moses, 1992, ^{1}H NMR relaxation and rock permeability: Geochimica et Cosmochimica Acta, **56**, 2947–2953.

Whittall, K. P., M. J. Bronskill, and R. M. Henkelman, 1991, Investigation of analysis techniques for complicated NMR relaxation data: Journal of Magnetic Resonance, **95**, 221–234.

Yaramanci, U., G. Lange, and M. Hertrich, 2002, Aquifer characterization using surface NMR jointly with other geophysical techniques at the Nauen/Berlin test site: Journal of Applied Geophysics, **50**, 47–65.

Yilmaz, A., M. Bucciolini, G. Longo, F. Franciolini, L. Ciraolo, and R. Renzi, 1990, Determination of dependence of spin-lattice relaxation rate in serum upon concentration of added Fe by MRI: Clinical Physics and Physiology Measurements, **11**, 343–439.